RSC Advances

ROYAL SOCIETY OF CHEMISTRY

www.rsc.org/advances

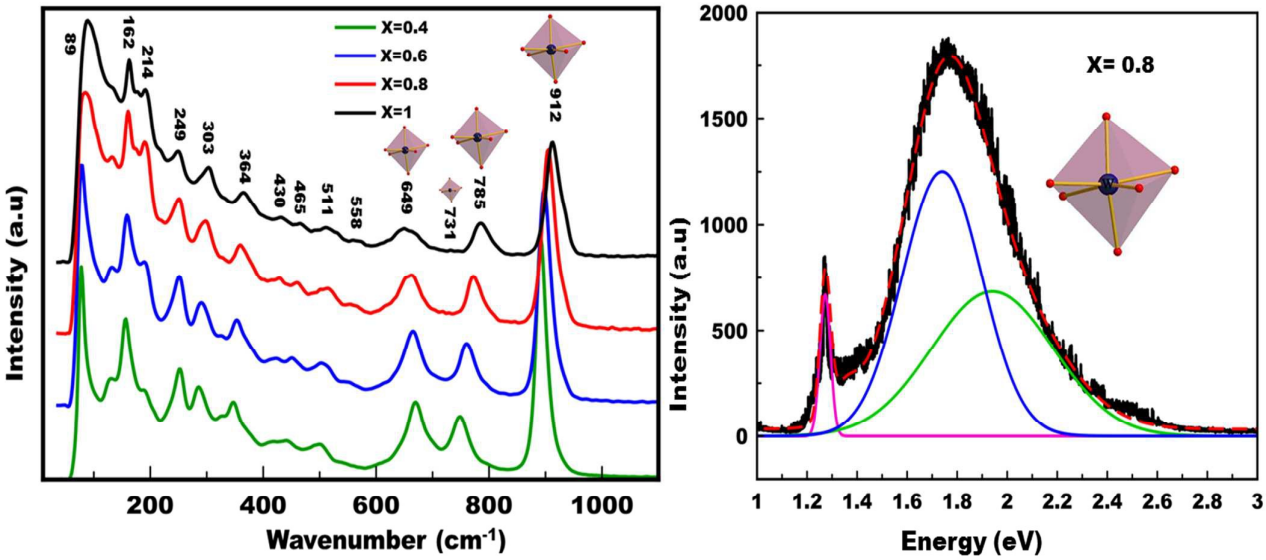

RSC Advances

Structural, vibrational study and UV photoluminescence properties of the system $Bi_{(2-x)}Lu_{(x)}WO_6$ $(0.1 \leq x \leq 1)$

H. Ait ahsaine[a*], M. Ezahri[a], A. Benlhachemi[a], B. Bakiz[a], S. Villain[b], J-C. Valmalette[b], F. Guinneton[b], M. Arab[b], J-R.Gavarri[b]

[a] Laboratoire Matériaux et Environnement LME, Faculté des Sciences, Université Ibn Zohr, BP 8106, Cité Dakhla, Agadir, Maroc

[b] Institut Matériaux Microélectronique et Nanosciences de Provence, IM2NP, UMR CNRS 6242, Université de Toulon, BP 20132, 83957, La Garde Cedex, France

(*) to whom correspondence must be addressed: H. Ait ahsaine: a.hassan@uiz.ac.ma

ABSTRACT

Bismuth lutetium tungstate series $Bi_{(2-x)}Lu_{(x)}WO_6$ with $0.1 \leq x \leq 1$ were synthesized by solid state reaction from oxide precursors, at 1000°C for 3 h. The as-prepared polycrystalline compounds were characterized by X-Ray Diffraction (XRD), scanning electron microscopy (SEM), Raman spectroscopy and photoluminescence (PL) analyses. Biphasic samples were obtained in the composition range $0.1 \leq x \leq 0.3$. Solid solutions were obtained in the composition range $0.4 \leq x \leq 1$, and their monoclinic crystal structure was refined using the Rietveld method. SEM micrographs showed that solid solutions presented homogeneous morphologies. Attributions of Raman vibrational modes were proposed. A shift in vibrational wavenumber depending on lutetium composition was observed. A specific broadening of spectral bands was interpreted in terms of long range Bi/Lu disorder and local WO_6 octahedron distortions in the structure. The PL experiments were performed under UV-laser light irradiation. Each PL band was decomposed into three gaussian components with energies close to 1.25, 1.80 and 2.1 eV. Their integrated intensities increased with composition x. The presence of the near infrared band at 1.25 eV is commented.

Key words: Bismuth lutetium oxides, Solid solution, X-Ray diffraction, Rietveld method, Raman spectroscopy, Photoluminescence.

I. INTRODUCTION

In the general framework of the development of multifunctional materials for various applications, we focus our attention on the correlations between structure and luminescence properties, in tungstate based materials. Generally, it is well established that extrinsic and intrinsic point defects can play a prominent role in photoluminescence properties.

Tungstate materials were extensively studied and investigated because of their potential applications in many fields as functional materials in high-performance luminescent materials [1-4], catalysts [5-6], scintillators[7], laser hosts[8] as well as microwave applications [9-10] and humidity sensors [11]. Metal tungstates with general formula AWO_4 can be divided into two groups, depending on tungsten environment: (i) scheelite-type structures with WO_4^{2-} tetrahedral groups and (ii) wolframite-type structures with WO_6^{6-} octahedral groups [12]. Depending on A^{2+} cation radii, $CaWO_4$ [13-14], $PbWO_4$ [15-16] and $AREWO_4$ (with A=alkali metal, RE= Rare earth element) [17-20] crystallize in the scheelite-type structures, whereas $CdWO_4$ [21], $ZnWO_4$ [22], $MgWO_4$ [23] and $BaWO_4$ [24] crystallize in the wolframite-type structures. Due to charge transfer linked to the tetrahedral or octahedral groups, tungstates can present interesting photoluminescence properties. Tungstates with the general formula RE_2WO_6 (RE= Y, La, Lu, Gd) belong to the second group with distorted WO_6 units and have attracted great attention in the field of luminescence [25].

Recently, lutetium-based compounds, such as Lu_2SiO_5 [26], $Lu_3Al_5O_{12}$[27], $LuAlO_3$ [28], $LuBO_3$ [29], Lu_2O_3 [30,31] and undoped and doped Lu_2WO_6 [32-34], have attracted increasing interest for their potential applications due to their excellent luminescence properties.

In our recent paper [35], we synthesized the new monoclinic compound Bismuth lutetium tungstate $BiLuWO_6$, with a structure similar to the one of the $BiREWO_6$ (RE= Rare Earth: Gd, Nd, Y) series. Its structure was characterized by a disorder due to the Bi/Lu bonding competition. In a previous work [36], we determined the local structure and the electrical properties of the layered phase Bi_2WO_6. In preliminary studies, we observed that, for compositions lower than x=0.1, a solid solution could be obtained with the orthorhombic structure of Bi2WO6. In an intermediate composition range, we observed a biphasic system with two structures similar to the ones of Bi_2WO_6 (orthorhombic) and $BiLuWO_6$

(monoclinic). Finally, for compositions x>0.35, we observed a unique monoclinic phase, similar to the one of $BiLuWO_6$.

In the present work, we investigate the system Bi_2WO_6-$BiLuWO_6$ represented by the general formula $Bi_{2-x}Lu_xWO_6$ with $0.1 \leq x \leq 1$. We use Rietveld method to refine the crystal structure of solid solutions with compositions $0.4 \leq x \leq 1$ and present the first vibrational analyses from Raman spectroscopy. Finally, we perform the first photoluminescence analyses under UV excitation as a function of composition x in lutetium.

II. EXPERIMENTAL SECTION.

Synthesis of the material. Bismuth lutetium tungstate compounds were prepared using solid state reaction process. To prepare $Bi_{(2-x)}Lu_{(x)}WO_6$ compounds, appropriate amounts of lutetium oxide Lu_2O_3 (Alfa Aesar Aldrich > 99%), bismuth oxide Bi_2O_3 (Fluka Chemika > 99%) and tungsten oxide WO_3 (Fluka Chemika > 99%), were mixed and milled in an agate mortar, as reported in our earlier paper [35]. Then, the mixture was heated at 1000°C for 15 hours.

X-Ray diffraction. The X-Ray diffraction (XRD) patterns were collected using an EMPYREAN PANALYTICAL diffractometer operating at 45 kV/35 mA, using CuKα radiation with Ni filter, and working in continuous mode with a step size of 0,013°. Data suitable for Rietveld refinement were collected over a range 5-90° in 2θ.

Microstructural characterization. Scanning electron microscopy (SEM) analyses were used to observe the morphology and the local composition of the polycrystalline material. The determination of chemical compositions was performed using Energy Dispersive Spectroscopy (EDS), in mode of sample surfaces scanning. Preliminary images were obtained with a SUPRA 40 VP COLONNE GEMINI ZEISS using a maximum voltage of 20 kV.

RAMAN spectroscopy. Raman spectra (RS) were recorded on a VERTEX 70 Raman spectrometer using a power of 30 mW and the wavelength of Ar green laser λ =514.5 nm. The frequency bands ν ranged from 50 to 1100 cm^{-1}.

UV Photoluminescence. The equipment used to perform the measurements of photoluminescence (PL) under UV excitation is a spectrometer Horiba Jobin-Yvon HR800 LabRam. The entrance slit, positioned behind the filter, is a diaphragm whose diameter can

range from 50 to 500 µm. The irradiated zone was limited to 1 µm in diameter for all samples. The polycrystalline samples were in form of compacted pellets obtained under a fixed pressure of 5 kbar. The spherical mirror, characterized by an 800 mm focal length, allows reflecting the scattered radiation from the input to the dispersive grating to obtain spectra slot. The **364.5 nm** (3.40 eV) line of an Ar-ion laser was used as the excitation source. The power applied to the samples was fixed to **0.005 mW** with an acquisition time set to **100 ms**.

III. RESULTS AND DISCUSSION

III.1. X-Ray Diffraction analyses

Figure 1 illustrates the XRD patterns of the synthesized compounds from x = 0.1 to x=1. A biphasic system is observed in the composition range $0.1 \leq x \leq 0.3$. Characteristic peaks of the orthorhombic bismuth tungstate Bi_2WO_6 were detected in addition to the peaks of the monoclinic structure $BiREWO_6$ (RE=Lu) phase. It should be recalled that all the as-prepared ceramics were thermally treated at 1000°C and were highly crystallized. The substituted compounds ranging from $0.4 \leq x \leq 1$ present a monoclinic structure and constitute a solid solution. This structural modification (orthorhombic/monoclinic) can be explained from the two electronic configurations of Bi^{3+} and Lu^{3+}: in the case of the Bi^{3+} cations (electron configuration $6s^2$ $6p^0$), the lone pair ($6s^2$) could play a spatial role in the structure organization, which is not the case for the Lu^{3+} cations. In addition, the ionic size of Lu^{3+} cations, smaller than the one of Bi^{3+} cations, argues in favor of the formation of a solid solution having the structure of the limit phase $BiLuWO_6$.

The identification of these compounds was firstly obtained from the standard JCPDS files (Joint Committee standards for Powder Diffraction) [37] in which the standard phases $BiYWO_6$, $BiNdWO_6$, $BiGdWO_6$ and H-Bi_2WO_6 were referenced. **Figure 2** shows that the diffraction peaks of the monoclinic solid solution are shifted to higher angles as x increases.

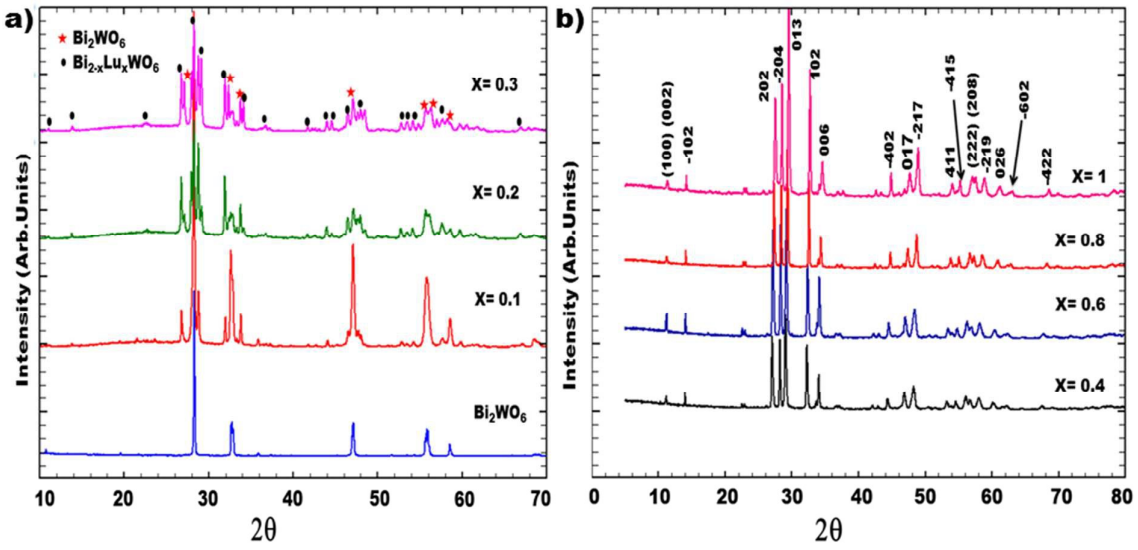

Figure 1: XRD pattern of the $Bi_{(2-x)}Lu_{(x)}WO_6$ obtained in room conditions : a) Biphasic system up to x=0.3; b) monoclinic solid solution up to x=1.

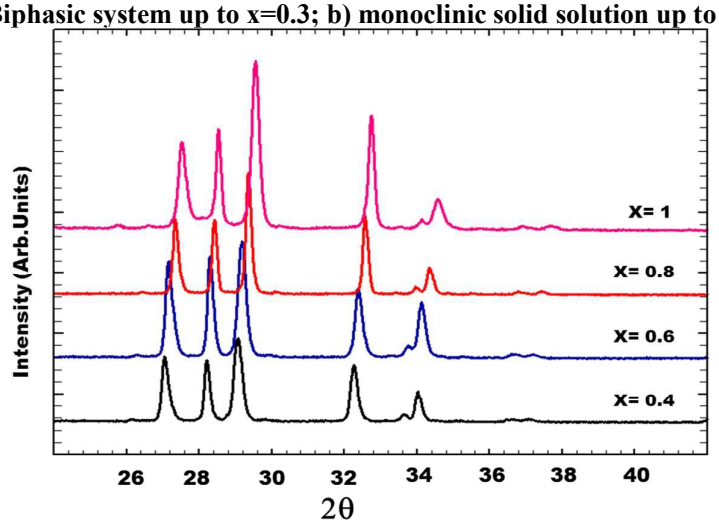

Figure 2: XRD patterns as a function of lutetium composition of the solid solution 0.4≤ x≤1.

The structural parameters of the solid solution ranging from 0.4≤ x≤1 were refined using FullProf suite software [38] which allows refinement of atomic coordinates, site occupancies and atomic displacement parameters as well as profile parameters (instrument parameters, background parameters, lattice constants and peak shape). The disordered model based on the work of Berdonosov and co-workers [39,40] on the series $Bi_{2-x}Ln_xWO_6$ (Ln=Lanthanide) was used in our Rietveld calculations. In this model, Lu atoms are assumed to be distributed on the two bismuth sites of the H-Bi_2WO_6 monoclinic structure characterized by a centrosymmetric A2/m space group. Such a substitution should involve specific

disordered distortions of the octahedral WO_6 groups, due to alternation of short Lu-O and long Bi-O bonds.

We refined the atom coordinates of the heavy atoms (Bi/Lu) and W, including their individual Debye factors and keeping fixed the oxygen coordinates, using a monoclinic A2/m space group. The occupancy factors of all atoms were fixed in agreement with the global composition x. We obtained a significant goodness of fit and the factors R_p, R_{exp}, R_{wp} and R_B are quite reliable. **Table 1a** reports the final calculated cell parameters for the solid solution samples. **Table 1b** reports the atom coordinates used for the refinement calculations. In the calculations, each (Bi,Lu) site is assumed to be occupied by Bi and Lu atoms in proportions corresponding to the composition x. The occupancy factors used in the Rietveld procedure are in an arbitrary scale.

Figure 3 shows the calculated and observed diffraction profiles $\mathbf{I_{obs}}$ **and** $\mathbf{I_{calc}}$ of the $Bi_{(1.2)}Lu_{(0.8)}WO_6$ compound. **Figure 4** shows the evolution and the influence of substitution of bismuth by lutetium on the cell parameters. The cell parameters a, b and c varies quasi-linearly with the composition x according, respectively, to the equations:

$$a(Å) = -0.1414x+8.2252 \ (R^2=0.999),$$

$$b(Å) = -0.0945x+3.8177 \ (R^2=0.997),$$

$$\text{and } c(Å) = -0.3467x+16.297 \ (R^2= 0.999).$$

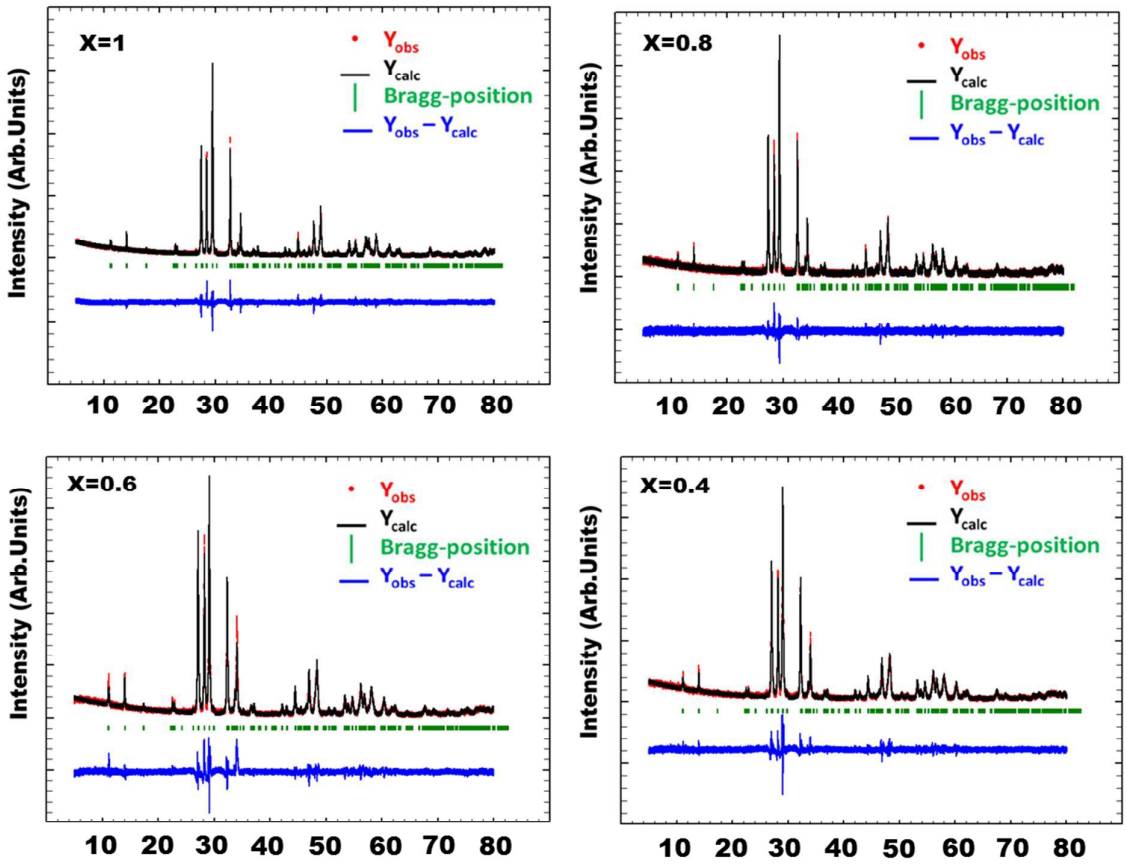

Figure 3: Rietveld refinement of $Bi_{2-x}Lu_xWO_6$ (x= 0.4; 0.6; 0.8 and 1) using disordered structure and space group A2/m.

Table 1a. Cell parameters and Debye-Waller factors for the solid solution compounds

	a (Å)	b (Å)	c (Å)	β(°)	B_{iso}(Bi/Lu)	B_{iso}(W)
$Bi_{1.6}Lu_{0.4}WO_6$	8.1683(2)	3.7797(1)	16.1564(3)	102.184(1)	0.28(3)	0.33(4)
$Bi_{1.4}Lu_{0.6}WO_6$	8.1403(2)	3.7619(3)	16.0923(3)	102.209(1)	0.57(4)	0.35(2)
$Bi_{1.2}Lu_{0.8}WO_6$	8.1134(1)	3.7405(3)	16.0202(2)	102.382(1)	1.11(3)	0.32(3)
$BiLuWO_6$ [34]	8.0830(1)	3.7238(1)	15.9493(2)	102.634(2)	0.72(3)	0.31(2)

Table 1b: atom coordinates (x, y, z, N) of (Bi,Lu) W and O atoms.

Compositions	Atom coordinates (x, y, z) and occupancy factors N (arbitrary scale)

		x	y	z	N(Bi) / N(Lu) N(W) or N(O)
x=1	Bi/Lu(1)	0.9224(2)	0.000	0.000 (2)	0.125 / 0.125
	Bi/Lu(2)	0.3960(2)	0.000	0.3170(2)	0.125 / 0.125
	W(1)	0.2951(3)	0.4792(3)	0.4925(3)	0.250
Reliability factors	R_p = 7% ; R_{exp} = 3% ; R_B = 4.99 % ; R_F = 4.74 %				
x=0.8	Bi/Lu(1)	0.9233(3)	0.000	0.3321(2)	0.150/0.100
	Bi/Lu(2)	0.3943(4)	0.000	0.3176(3)	0.100/0.150
	W(1)	0.2960(2)	0.4450(2)	0.4970(3)	0.250
Reliability factors ([a])	R_p = 8.35% ; R_{exp} = 7.73% ; R_B = 6.20% ; R_F = 4.72%				
x=0.6	Bi/Lu(1)	0.9266(3)	0.000	0.3327(2)	0.175/0.075
	Bi/Lu(2)	0.3929(2)	0.000	0.3189(2)	0.075/0.175
	W(1)	0.3020(2)	0.4485(3)	0.4994(2)	0.250
Reliability factors ([a])	R_p = 9.21% ; R_{exp} = 6.79% ; R_B = 7.43% ; R_F = = 5.48%				
x=0.4	Bi/Lu(1)	0.9277(2)	0.000	0.3331(3)	0.200/0.050
	Bi/Lu(2)	0.3950(3)	0.000	0.3183(2)	0.05/0.200
	W(1)	0.2985(3)	0.4560(3)	0.4990(4)	0.250
Reliability factors ([a])	R_p = 9% ; R_{exp} = 7.87% ; R_B = 5.46% ; R_F 5.24%				
Fixed Oxygen atoms	*O(1)*	*0.1188*	*0.000*	*0.2489*	*0.250*
	O(2)	*0.3640*	*0.500*	*0.2338*	*0.250*
	O(3)	*0.3224*	*0.000*	*0.5284*	*0.125*
	O(4)	*0.5068*	*0.438*	*0.5745*	*0.250*
	O(5)	*0.1709*	*0.414*	*0.5669*	*0.250*

	O(6)	*0.1664*	*0.609*	*0.3992*	*0.250*
	O(3a)	*0.2978*	*0.000*	*0.4628*	*0.125*

([a]) Note on the reliability factors :

$R_p = 100. \{\sum | y_i^{obs} - y_i^{calc} | / \sum | y_i^{obs} |\}$

$R_{exp} = 100. \{[(N-P+C) / \sum w_i | y_i^{obs} |^2]^{1/2} \}$

$R_B = 100. \{\sum | I_k obs - I_k calc | / \sum | I_k obs |\}$

$R_F = 100. \{\sum | F_k obs - F_k calc | / \sum | F_k obs |\}$

Where N, P and C are the number of observations, parameters and constraints, respectively.

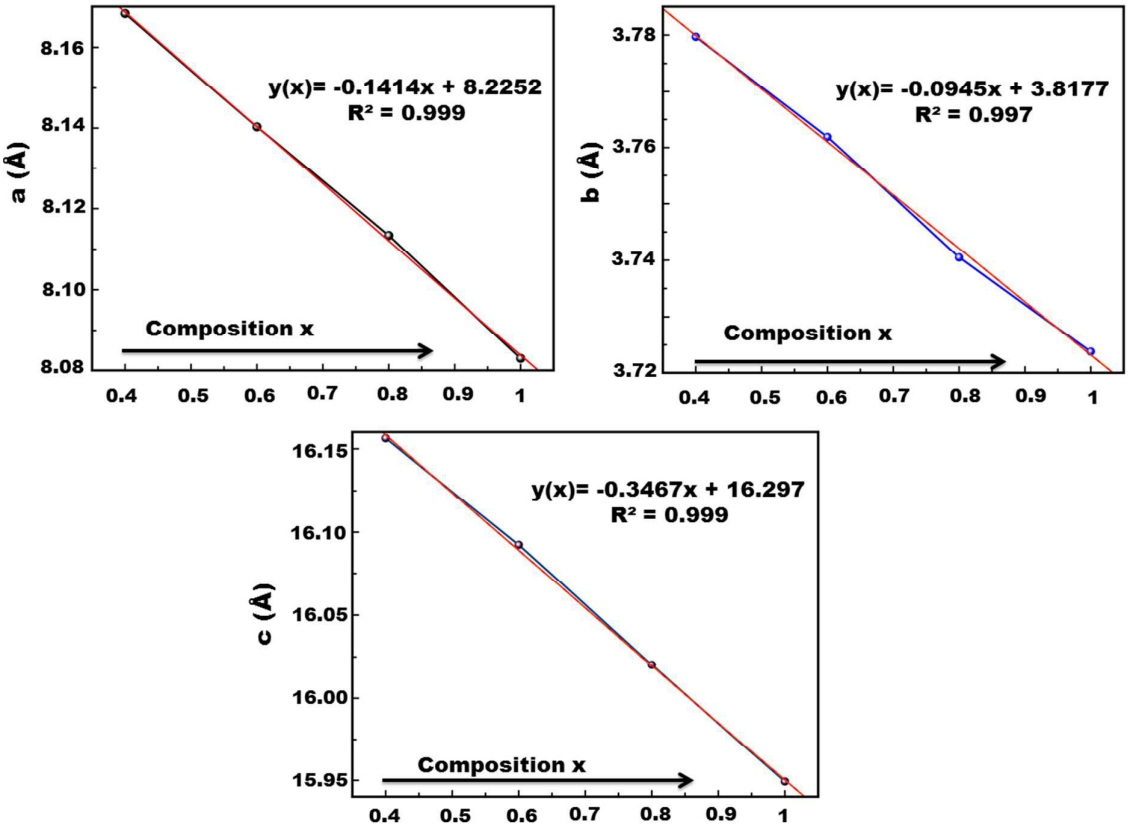

Figure 4: Evolution of cell parameters as a function of Lutetium fraction x.

The Debye-Waller factor B of (Bi,Lu) site increases as x increases, with an apparent maximum value at x=0.8 (**Figure 5**). Having regard to the standard deviations (close to 10%) of these B values, this increase can be ascribed to the existence of increasing local distortions involved by the disorder on the (Bi/Lu) site. The disorder can be illustrated by the alternation of different chemical bonds Bi-O and Lu-O, as discussed in references [35,39,41].

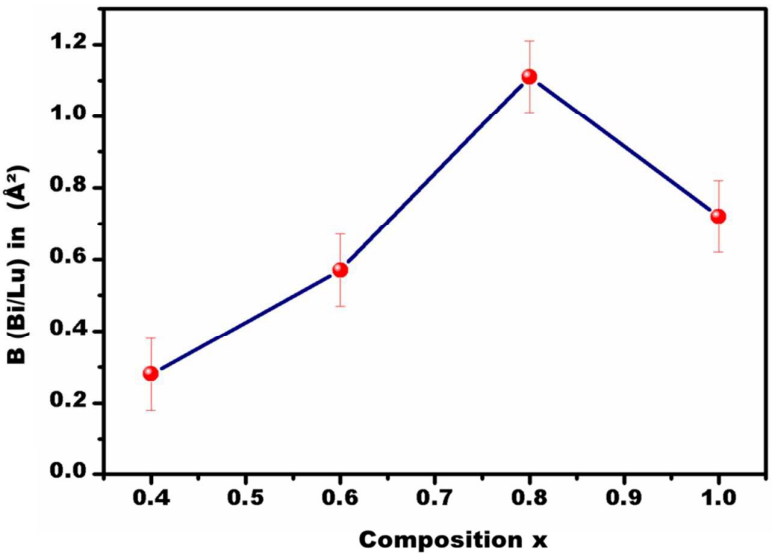

Figure 5: Evolution of Debye-Waller factor B of (Bi,Lu) site as a function of x.

The monoclinic structure of bismuth lutetium tungstates can be considered as being close to a wolframite-type structure. **Figure 6** shows the alternating $(Bi,Lu)_2O_2$ layers and the WO_6 edge sharing octahedra. Crystallographic data obtained from our Rietveld calculations showed that the WO_6 octahedral complexes have irregular shapes with short, medium and long bonds ranging from 1.65 Å to 2.13 Å.

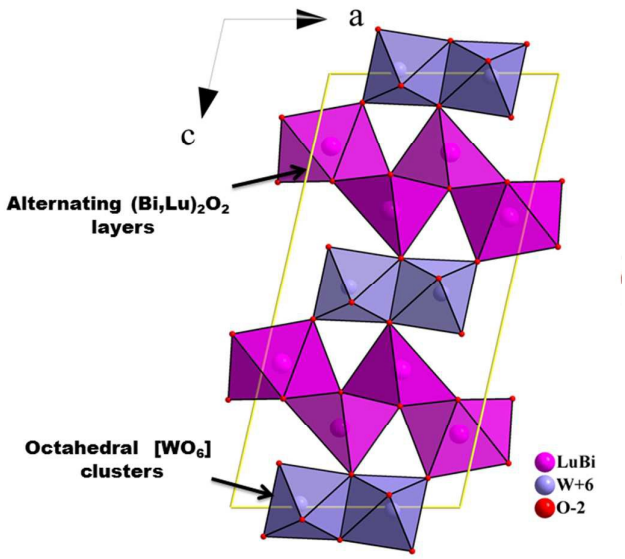

Figure 6: Crystal structure of monoclinic $Bi_{2-x}Lu_xWO_6$ compounds in the (010) plane.

III.2. Scanning electron microscopy

The SEM micrographs reported in **Figure 7** show the morphology of the synthesized $Bi_{(2-x)}Lu_{(x)}WO_6$:

- In the range of $0.1 \leq x \leq 0.3$, the samples present two types of grain morphologies, with small grains similar to the ones observed in the pure Bi_2WO_6 samples and micrometric grains similar to the ones observed in the monoclinic samples ($0.4 \leq x \leq 1$): these two aspects are compatible with the XRD analyses showing the presence of two phases.
- In the solid solution range $0.4 \leq x \leq 1$, the morphology is quite uniform and consists of rounded shaped grains having dimensions of 1 to 2 μm, as shown in the inset micrographs.

The EDS microanalysis is congruent with the nominal chemical composition in heavy atoms of $Bi_{(2-x)}Lu_{(x)}WO_6$ and no significant variation in composition can be observed at a local scale. **Table 2** reports the theoretical and the experimental composition of the as synthesized samples (O atoms were excluded during the EDS analysis). Each EDS experimental fraction is determined with a standard deviation of about 2%.

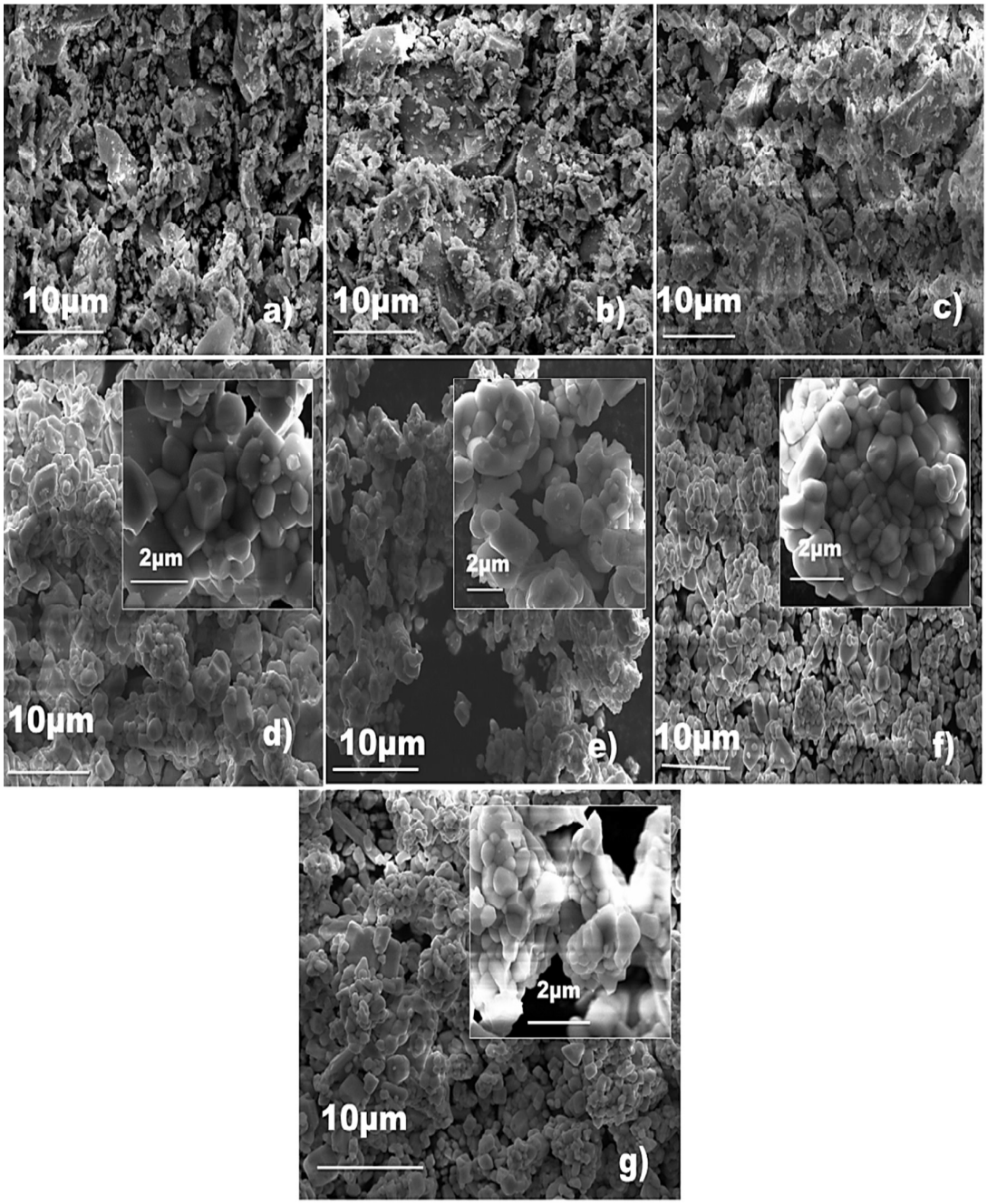

Figure 7: SEM micrographs of the as-synthesized samples:
Biphasic samples: a) x=0.1, b) x=0.2, c) x=0.3
Solid solutions (with in inset regular rounded shapes):
d) x=0.4, e) x=0.6, f) x=0.8, g) x=1.

Table 2: Theoretical and experimental composition from EDS analysis

Compound	Theoretical compositions in at.%	EDS analyses in at.% (*)
x=0.1	Bi (63.33), Lu (3.33), W (33.33)	Bi (64), Lu (3), W(33)
x=0.2	Bi (60.00), Lu (6.66), W (33.33)	Bi (59), Lu (8), W(33)
x=0.3	Bi (56.66), Lu (10.00), W (33.33)	Bi (57), Lu (10), W(33)
x=0.4	Bi (53.33), Lu (13.33), W (33.33)	Bi (53), Lu (14), W(33)
x=0.6	Bi (46.66), Lu (20.00), W (33.33)	Bi (46), Lu (20), W(34)
x=0.8	Bi (40.00), Lu (29.33), W (33.33)	Bi (40), Lu (27), W(33)
x=1	Bi (33.33), Lu (33.33), W (33.33)	Bi (33), Lu (33), W(34)

(*) Note : Statistical deviations (in %) on Bi, Lu and W compositions are of about : Bi (2 to 4 %) / Lu (4 to 15%) / W (4%). Determination from series of surface analyses.

III.3. Raman spectroscopy analyses

In the case of $Bi_{2-x}RE_xWO_6$ structures, detailed attributions of vibration modes were previously proposed by authors G.N Rocha et al. [42] for the bismuth rare earth monoclinic compounds (RE = Y, Nd, Gd). The irreducible representation, for these structures, is as follows:

$$\Gamma = 24A_g + 18A_u + 18B_g + 24B_u \text{ (44 active Raman modes)}$$

Generally, these Raman modes (i.e $\mathbf{A_g}$ and $\mathbf{B_g}$) can be classified into four categories: (i) symmetric and asymmetric stretching vibrations of the WO_6 octahedrons, (ii) bending vibrations of the WO_6, (iii) stretching and bending vibrations of the $(Bi_2O_2)^{2+}$ layers, and (iv) vibrations involving translational motions of Bi^{3+} /Lu^{3+} and W^{6+} ions.

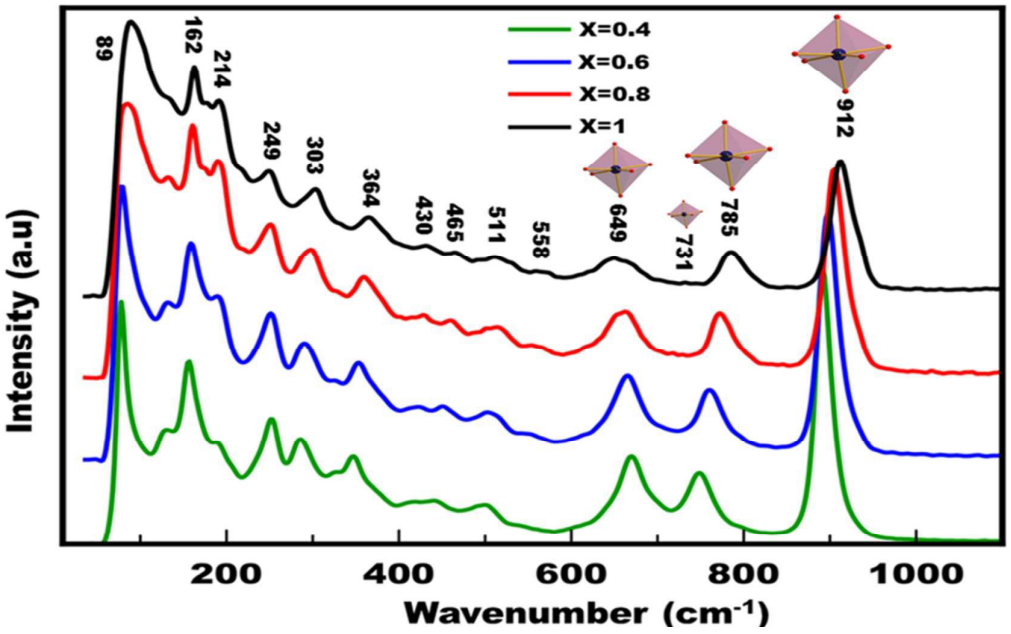

Figure 8: Raman spectra (λ=514.5 nm) of the solid solution $Bi_{(2-x)}Lu_{(x)}WO_6$ (0.4≤x≤1).

Figure 8 presents the vibrational bands of the compounds belonging to the composition range **(0.4≤x≤1)** : all the compounds exhibit the same vibrational band profiles with a shifting to higher wavenumbers as the composition of lutetium x increases. **Table 3** reports the assignments of the Raman bands of the solid solution and the Full width at Half Maximum (FWHM) of each composition. As lutetium composition x increases, we observe increasing wavenumbers and broadenings (FWHM) of all vibration bands. This can be ascribed to the increasing population of Lu-O bonds having stronger force constants with increasing distortions due to the disordered distributions of Lu-O and Bi-O bonds.

Table 3: Raman spectroscopy data and assignments of vibration bands for the solid solution (0.4≤x≤1). Wavenumbers (ν) and full width at half maximum (FWHM) in cm^{-1}.

Wavenumbers (FWHM)				Assignments [**42**]
x=0.4	x=0.6	x=0.8	x=1 [**35**]	
891 (20)	897 (25)	905 (30)	912 (40)	Asymmetric stretching of WO_6 (Apical O)
750 (30)	762 (27)	770 (20)	785 (30)	symmetric stretching of WO_6 (Apical O)
__	708 (--)	729 (3)	731 (5)	

667(20)	664(18)	665(20)	670 (22)	Asymmetric stretching of WO_6 (Equatorial O)
___	__	647 (-)	649 (22)	
544 (12)	550 (10)	554 (19)	558 (20)	Bending of WO_6 and stretching + bending of $(Bi,Lu)O_6$ polyhedra
500 (22)	504 (30)	509 (27)	511 (20)	
440 (--)	451(9)	459 (10)	465 (15)	
413 (--)	417 (10)	428 (10)	430 (16)	
347 (18)	353 (15)	359 (17)	364 (15)	Remaining bending of the octahedral Oxygen and Bi_2O_3 layers
286 (21)	289 (19)	299 (20)	303 (12)	
251 (21)	251 (22)	249 (20)	249(20)	
___	__	___	214 (--)	
189 (11)	189 (10)	189 (8)	191(10)	
154 (16)	158 (18)	160 (17)	162(15)	Translation of Bi^{3+}/Lu^{3+} and W^{6+} ions
77 (21)	77 (25)	83 (27)	89 (35)	Lattice modes

The vibrational motions of WO_6 octahedra and $(Bi/Lu)_2O_2$ layers are directly perturbed by the disorder of Bi-O and Lu-O bonds conditioned by the increasing composition of lutetium, involving increasing disorder in oxygen positions of WO_6 octahedra. This should be a major argument for the disorder model used in the Rietveld refinements to interpret our XRD data. As already reported for the $BiLuWO_6$ sample, the Raman bands can be highlighted as follows:

- The Raman peaks at 904 and 760 cm^{-1} can be ascribed to the symmetric and antisymmetric stretching modes of the octahedra WO_6, which involve the apical motion of oxygen atoms perpendicular to the layers.
- The peaks in the region of 720-640 cm^{-1} can be associated to the asymmetric stretching of octahedra involving equatorial motions of oxygen atoms within layers [43-47].
- The bands in the mid-region 370-589 cm^{-1} represent the bending modes of WO_6 and stretching-bending modes of $(Bi, Lu)O_n$.
- Some bands are well defined in the spectral range 180-370 cm^{-1} and are related to bending modes of the oxygen in Bi-O polyhedra of the Bi_2O_2 layers.
- The bands below 180 cm^{-1} can be ascribed to the translation of Bi^{3+}/Lu^{3+} and W^{6+} ions [43,48,49].

III.4. Photoluminescence properties

By the past, the luminescence in scheelite tungstates was interpreted in terms of electronic charge transfers in the WO_4^{2-} complex oxyanions or in WO_3 defect centers [50]. Using a molecular orbital model for the octahedral WO_6^{6-} oxyanion, Von Oostehort et al. [51] showed that the excited state consisted of an electron initially on an oxygen 2p orbital (O2p) and occupying the tungsten 5d orbitals (W5d) with t_{2g} symmetry. Following this model, the emission spectra imply transitions starting from the double triplet $^3T_{1u}$ levels to the ground $^1A_{g1}$ level. Other authors [52-55] proposed similar interpretations : some of them described the basic emissions through transitions from two triplet states $^3T_1$ and $^3T_2$ to ground state $^1A_1$ in the case of scheelite structures (charge transfer in WO_4^{2-} oxyanions), or from two triplet states $^3T_{1u}$ and $^3T_{2u}$ to ground state $^1A_{1g}$ in the case of wolframite structures (charge transfer in WO_6^{6-} oxyanions). In the case of octahedral WO_6^{6-} oxyanions, two additional transitions corresponding to weaker energies were also envisaged. Recently, in our work on $Ca_{1-x}Cd_xWO_4$ solid solutions [56], we observed photoluminescence bands under UV excitation localized in the approximate energy range 2.1 to 2.7 eV.

In the case of bismuth based compounds, the photoluminescence signals under UV excitations were previously ascribed to internal bismuth transitions [57]: authors used theoretical calculations to justify emissions with wavelengths ranging between UV-visible range of 300 to 600 nm, and near infrared (NIR) emissions with wavelengths observed in the approximate range 800 nm to 1500 (and above) nm. NIR emissions were frequently observed in various bismuth doped materials including glasses [58,59]. These NIR emissions depended on the excitation energies and on the host material itself. The origins of these emissions are unclear today. According to these authors, these emissions could be generated by bismuth species such as Bi^{2+}, Bi^{+} or BiO molecules as probable defect centers (the list of the possible defect centers is not clearly limited by the authors).

The photoluminescence bands obtained under UV excitation (energy of 3.40 eV) are reported on **Figure 9**. The emission bands present energies ranging between 1.1 and 2.8 eV. The PL bands have been decomposed into three Gaussian components (G1, G2, G3). The resulting fit is quite satisfactory. The multi-Gaussian decomposition analyses are shown in **Figure 9**. **Table 4** gives the characteristics of the fitted gaussian functions: energies of maximum, integrated intensities and FWHM.

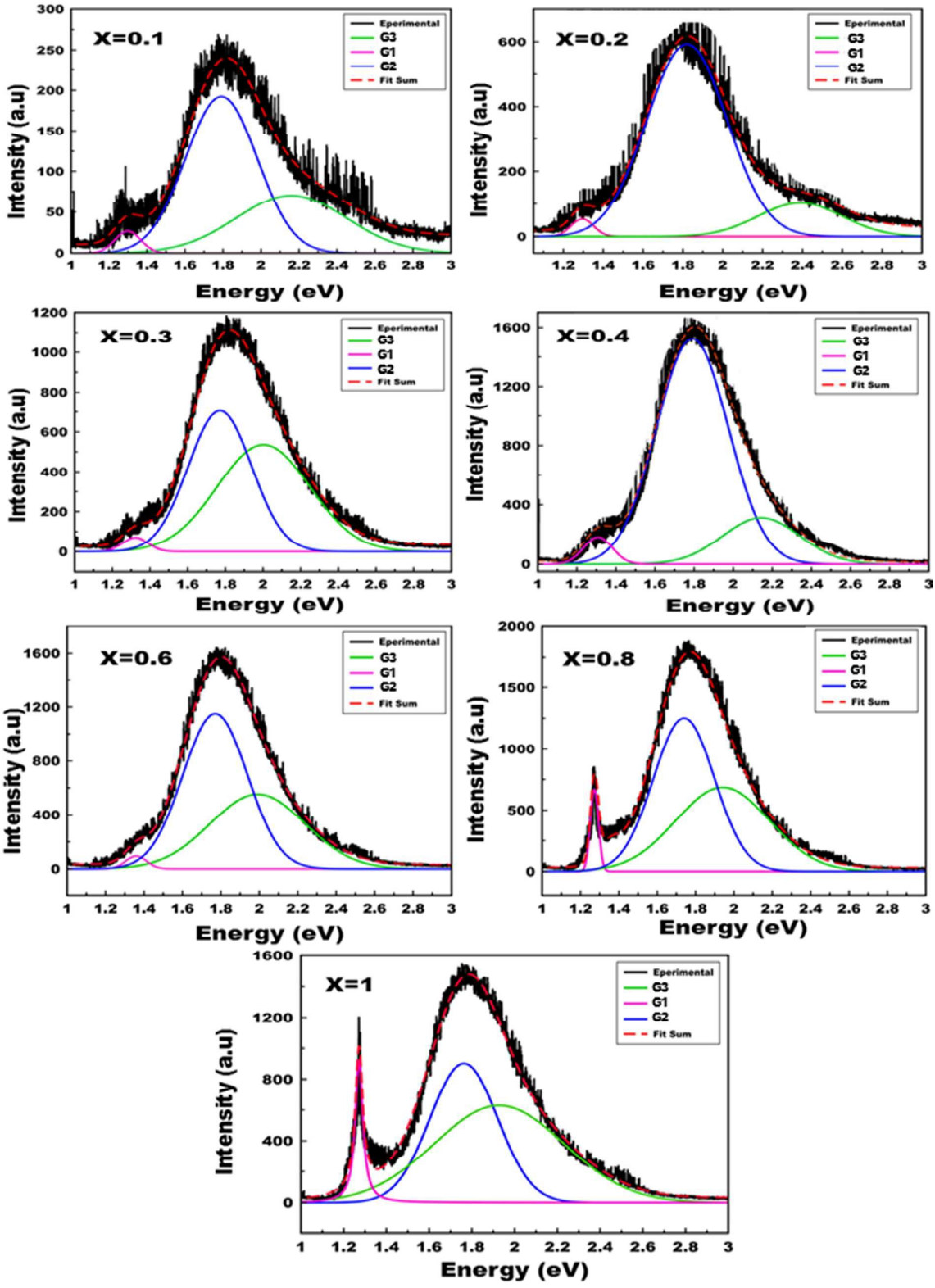

Figure 9: Luminescence spectra of the polycrystalline $Bi_{(2-x)}Lu_{(x)}WO_6$ phosphors with $0.1 \leq x \leq 1$, three Gaussian components are shown in each figure.

Table 4: the characteristics of the fitted gaussian functions: energies of maximum, integrated intensities and FWHM

		energies of maximum (eV)	integrated intensity (a.u)	FWHM (eV)
X=0.1	**G1**	1.279	26.8	0.08
	G2	1.791	192.3	0.22
	G3	2.160	70.1	0.34
X=0.2	**G1**	1.295	53.7	0.07
	G2	1.779	475.8	0.20
	G3	2.101	161.2	0.37
X=0.3	**G1**	1.322	69.6	0.08
	G2	1.778	770.2	0.21
	G3	2.022	460.0	0.29
X=0.4	**G1**	1.321	125.4	0.09
	G2	1.781	1117.6	0.20
	G3	1.967	546.9	0.31
X=0.6	**G1**	1.359	127.3	0.08
	G2	1.770	1128.7	0.21
	G3	1.971	527.3	0.29
X=0.8	**G1**	1.272	669.1	0.02
	G2	1.739	1250.4	0.19
	G3	1.941	684.3	0.29
X=1	**G1**	1.272	924.5	0.02
	G2	1.762	901.7	0.19
	G3	1.927	627.7	0.36

In **Figure 10**, each Gaussian is characterized by its intensity and its energy as a function of the composition x. The energies of the components G1 (close to 1.27eV) and G2 (close to 1.78eV) are quasi-independent of the composition x. As x increases, G3 presents a shifting to lower energies from 2.16 eV to 1.92 eV.

The G1 component appears as being a narrow band for high lutetium content, strongly related to the increasing lutetium composition. The origin of the G1 component seems to be unclear: as it has a low energy, H. Wang et al [60] in their study on $ZnWO_4$ interpreted a broad emission band close to 990 nm (with wavelengths ranging between 850 and 1100 nm), as being related to the presence of defect centers due to oxygen vacancies. In other terms, their broad NIR signal would be related to defect centers on the WO_6^{6-} groups. However, in our case, the emission band G1, observed at 991 nm or 1.27 eV, is a narrow band. As the intensity of our G1 emission band is strongly conditioned by the lutetium composition, a different interpretation might be proposed. This narrow band could result from a transition due to specific bismuth species acting as defect centers as previously suggested [57,58]: in the case of increasing lutetium composition, these bismuth species should appear as more isolated defects giving rise to high sensitization under UV excitation. For low concentration of lutetium, the low intensity of this G1 component might result from a quenching effect. For high lutetium fractions i.e. lower fraction of bismuth, this quenching effect might decrease.

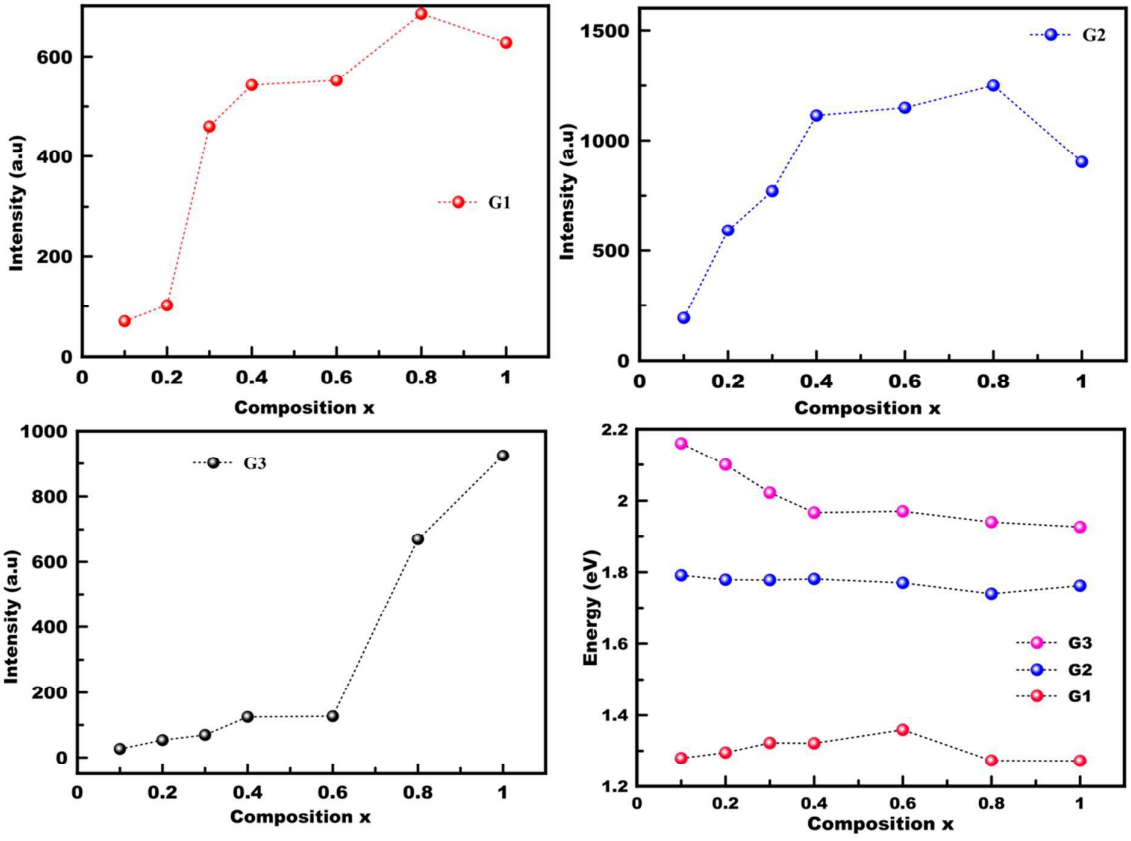

Figure 10: Integrated intensities and centroid energies of the three Gaussians as a function of lutetium composition.

The high energetic component G2, which has a maximum at x=0.8, is attributed to the allowed transition $^1T_{1u} \rightarrow {}^1A_{1g}$ of the tungstate groups. Whereas the G3 component presents the same behavior as the G2, it increases with x till a maximum at x =0.8, this component could be linked to the $^3T_{1u} \rightarrow {}^1A_g$ transitions.

The integrated intensities of the experimental data are shown in **Figure 11**. It should be noted that the intensities of all components increase strongly in the composition range $0.1 \leq x \leq 0.4$ corresponding to the biphasic system. The total intensity (G1+G2+G3) is quasi-constant for compositions x>0.4 corresponding to the solid solutions, despite the fact that the intensity of the small G1 component increases slowly as x increases. In the biphasic system, this can be due to the progressive formation of the second (Bi-Lu) phase coexisting with the inactive Bi_2WO_6 phase, while, in the (Bi-Lu) monoclinic solid solution, the activation of luminescence (G1, G2 and G3 components) should occur. As the G2 and G3 intensities remain quasi-constant, this luminescence could be ascribed to charge transfers (or defect centers) linked to the WO_6 groups of the monoclinic structure.

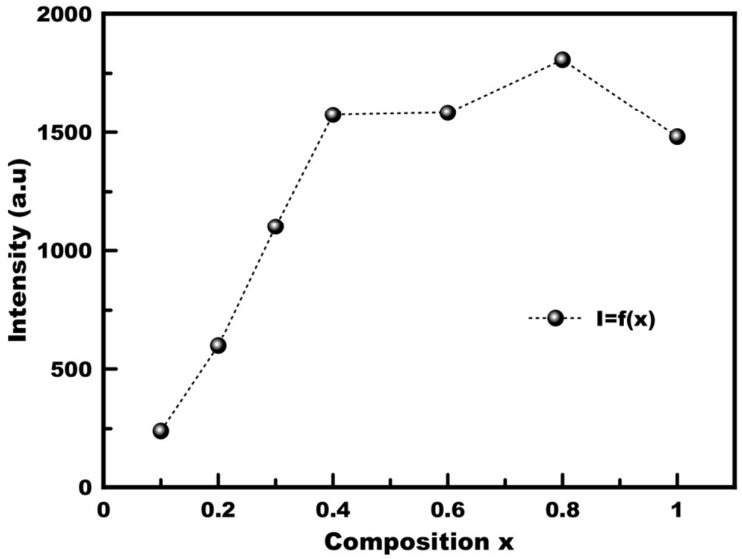

Figure 11: Experimental Integrated intensities as function of composition x.

CONCLUSION

In this study, we have investigated the complex tungstate system (1-x)Bi_2WO_6-x$BiLuWO_6$ or $Bi_{2-x}Lu_xWO_6$ and observed the existence of a mix system for $x<0.4$ and a solid solution for $0.4\leq x\leq 1$. Rietveld refinements of the monoclinic structures of the solid solution system showed that the Lu^{3+} cations are distributed on the Bi sites. X-ray diffraction analyses coupled with Raman spectroscopy results showed the existence of disordered distributions of Lu and Bi atoms, associated with local distortions.

The photoluminescence under monochromatic UV excitation seems to be strongly related to the formation of the monoclinic structure induced by the substitution of bismuth by lutetium. It has been decomposed into two types of emissions: the classical emission of tungstate groups WO_6^{6-} with two components due to charge transfers "W5d ➔ O2p" in the case of octahedral coordination, and a specific emission (narrow band at 1.25 eV) strongly related to the presence of lutetium. The exact origin of this NIR emission is not clearly established. If we refer to literature results on tungstates, this NIR emission might be due to defect centers due to oxygen vacancies or defect centers due to bismuth species with different valences or different molecular clustering.

Acknowledgments: A part of this work was financially supported by the CNRS-CNRST project N° 0749/14, by the Regional Council of Provence-Alpes-Côte d'Azur, by the General Council of Var and by Toulon Provence Mediterranean.

REFERENCES

1. H.Y. Li, H.K. Yang, B.K. Moon, B.C. Choi, J.H. Jeong, K. Jang, H.S. Lee, S.S. Yi, ,J. Alloys Compd., 2011, 509, 8788–8793

2. H.Y. Li, H.K. Yang, B.K. Moon, B.C. Choi, J.H. Jeong, K. Jang, H.S. Lee, S.S. Yi,Inorg. Chem., 2011, 50, 12522–12530

3. V.S. Marques, L.S. Cavalcante, J.C. Sczancoski, A.F.P. Alcantara, M.O. Orlandi, E. Moraes, E. Longo, J.A. Varela, M.S. Li, M.R.M.C. Santos, ,Cryst. Growth Des., 2010, 10, 4752–4768

4. W. Zhang, J. Long, A. Fan, J. Li, , Mater. Res. Bull., 2012, 47, 3479–3483

5. A.Kudo, Y. Miseki, Chem. Soc. Rev., 2009, 38, 253–278

6. K. Kamata, T. Kimura, H. Sunaba, N. Mizuno, ,Catal. Today, 2014, 226, 160–166

7. L. Huo, Y. Chu,, Mater. Lett., 2006, 60 , 2675–2681

8. H. Zhao, J. Wang, J. Li, H. Zhang, J. Zhang, Z. Ling, H. Xia, R.I. Boughton, ,Mater. Lett., 2007, 61, 2499–2501

9. J.C. Sczancoski, L.S. Cavalcante, M.R. Joya, J.A. Varela, P.S. Pizani, E. Longo, J. Chem. Eng, 2008, 140, 632–637

10. J. Liu, J. Ma, B. Lin, Y. Ren, X. Jiang, J. Tao, X. Zhu, , Ceram. Int., 2008, 34, 1557–1560

11. T. Thongtem, A. Phuruangrat, S. Thongtem, J. Ceram. Process. Res. 2008, 9, 258–261.

12. J. Ungelenk, M. Speldrich, R. Dronskowski, C. Feldmann, Solid State Sci., 2014, 31, 62–69

13. V.B. Mikhailik, H. Kraus, G. Miller, M.S. Mykhaylyk, D. Wahl, J. Appl. Phys., 2005,97, 083523

14. Y.G. Su, L.P. Li, G.S. Li, Chem. Mater., 2008, 20, 6060–6067

15. J. Yang, C. Lu, H. Su, J. Ma, H. Cheng, L. Qi, Nanotechnology, 2008,19, 035608

16. X.L. Hu, Y.J. Zhu, Langmuir, 2004, 20, 1521–1523

17. F. Lei, B. Yan, H.H. Chen, J.T. Zhao, Inorg. Chem., 2009, 48, 7576–7584

18. W. Bolanos, J.J. Carvajal, M.C. Pujol, X. Mateos, G. Lifante, M. Aguilo, F. Diaz, Cryst. Growth Des., 2009, 9, 3525–3531

19. F. Esteban-Betegon, C. Zaldo, C. Cascales, Chem. Mater., 2010, 22, 2315–2324

20. F. Wang, X.P. Fan, D.B. Pi, Z.Y. Wang, M.Q. Wang, J. Solid State Chem., 2005, 178, 825–830

21. Y. Abraham, N.A.W. Holzwarth, R.T. Williams, Phys. Rev. B, 2000, 62, 1733–1741

22. H. Ait ahsaine, A. Taoufyq, M. Ezahri, A. Benlhachemi, B. Bakiz, S. Villain, M. Arab, F. Guinneton, J-R gavarri, J. Mater. Environ. Sci., 2014, 5, 2449-2454

23. S. Wannapop, T. Thongtem, S.Thongtem, Appl. Surf. Sci., 2012, 258, 4971–4976

24. W.M. Chance, M.D. Smith, H.C. zur Loye, J. Chem. Crystallogr., 2014, 44, 20–24

25. Xiang-Yang Chen, Zhi-Jun Zhang, Ang Feng, Meng Xu, Jing-Tai Zhao, Fang-Fang Xu, Mater. Res. Bull., 2015, 70, 26-31

26. M. Zhuravleva, S. Friedrich, C.L. Melcher, Appl. Phys. Lett., 2012, 101, 101902

27. Y. Zorenko, V. Gorbenko, I. Konstankevych, A. Voloshinovskii, G. Stryganyuk, V. Mikhallin, V.

Kolobanov, D. Spassky, J. Lumin., 2005, 114, 85–94

28. D. Singh, Phys. Rev. B, 2007, 76, 214115

29. B.I. Zadneprovski, V.V. Sosnovtsev, D.G. Permenov, A.A. Meotishvili, G.I. Voronova, Tech. Phys. Lett., 2009, 35, 815–818

30. N. Kalyvas, P. Liaparinos, C. Michail, S. David, G. Fountos, M. Wójtowicz, E. Zych, I. Kandarakis, Appl. Phys. A, 2011, 106, 131–136

31. H. Ait ahsaine, L. Atourki, M. Ezahri, K. Bouabid, A.Ihlal, S. Villain, A. Benlhachemi, Mater. Lett. 2015, 160, 415-418

32. A. Madej, M.E. Witkowski, A.J. Wojtowicz, E. Zych, J. Lumin. 2015, 160, 50-56

33. X-Y. Chen, Z-J. Zhang, L-L. Zhu, M. Xu, H. Wang, A-G. Li, J-T. Zhaoc, Appl. Surf. Sci., 2014, 317, 730-736

34. Z. Zhang, H. Zhang, Ch. Duan, J Yuan, X Wang, D. Xiong, H. Chen, J. Zhao, J. Alloys Compd., 2008, 466, 258

35. H. Ait ahsaine, A. Taoufyq, L. Patout, M. Ezahri, A. Benlhachemi, B. Bakiz, S. Villain, F. Guinneton, J-R Gavarri, J. Solid State Chem, 2014, 218, 124-130

36. A. Taoufyq, H. Ait ahsaine, L. Patout, A. Benlhachemi, M. Ezahri, F. Guinneton, A. Lyoussi, G. Nolibe, J-R. Gavarri, J. Solid. Stat. Chem. 2013, 203, 8-18

37. Powder Diffraction File PDF data base sets. JCPDS, International Center for Diffraction Data. Swathmore, P.A, U.S.A. (1994).

38. J. Rodriguez-Carvajal Comission Powder Diff. Int. Union Cryst., Newsletter, 2001, 26, 12–19.

39. P. S. Berdonosov, D. O. Charkin, K. S. Knight, K. E. Johnston, R. J. Goff, V. A. Dolgikh, P. Lightfoot, J. Solid State Chem. 2006, 179, 3437-3444.

40. P. S. Berdonosov, D. O. Charkin, V. A. Dolgikh, S. Yu Stefanovich, R. I. Smith, P. Lightfoot, J. Solid State Chem. 2004, 177, 2632–2634

41. A. Watanabe, Y. Sekikawa, F. Izumi, J. Solid State Chem., 1982, 41, 138

42. G.N. Rocha , L.F.L. Melo , M.C. Castro Jr. , A.P. Ayala , A.S. de Menezes, P.B.A. Fechine J. Phys. Chem., 2010, 71, 579-582.

43. M. Maczka, L. Macalik, K. Hermanowicz, L. Kepinski, P. Tomaszewski, J. Raman Spectrosc., 2010, 41, 1059–1066.

44. M. Maczka, L. Macalik, S. Kojima, J. Phys. Condens. Matter. 2011, 23, 405902.

45. H.C. Gupta, V. Archana, Luthra, J. Mol. Struct. 2011, 1005, 53–58.

46. M. Maczka, L. Macalik, J. Hanuza, J. Raman Spectrosc., 2009, 40, 2099–2103.

47. M. Maczka, J. Hanuza, W. Paraguassu, A.G. Souza Filho, P.T.C. Freire, J. Mendes Filho, J. Appl. Phys. Lett., 2008, 92, 112911.

48. H. Huang, H. Chen, Y. Xia, X. Tao, Y. Gan, X. Weng, W. Zhang, J. Colloid Interface Sci., 2012, 370 , 132–138.

49. L.W. Zhang, Y.J. Wang, H.Y. Cheng, W.Q. Yao, Y.F. Zhu, J. Adv. Mater., 2009, 21, 1286–1290.

50. V. Nagirnyi, E. Feldbach, L. Jönsson, M. Kirm, A. Lushchik, Ch. Lushchik, L. L. Nagornaya, V. D. Ryzhikov, F. Savikhin, G. Svenson, I. A.Tupitsina, Radiat. Meas., 1998, 29 , 247-250

51. A. B. J. von Oosterhout, Chem. Phys. 1977, 67 , 2412-2418

52. V.B. Mikhailik, H. Kraus, G. Miller, M.S. Mykhaylyk, D. Wahl, J. Appl. Phys., 2005, 97, 083523

53. V. Nagirnyi, E. Feldbach, L. Jonsson, M. Kirm, A. Kotlov, A. Lushchik, V.A. Nefedov, B.I. Zadneprovski, Nucl. Instrum. Meth. A ., 2002, 486 (1), 395-398.

54. A.E. Ovechkin, V.D. Ryzhikov, G. Tamulaitis and A. Žukauskas, J. Phys. status solidi A., 1987, 103 (1), 285-290.

55. R. Grasser, E. Pitt, A. Scharmann, G. Zimmerer, J. Phys. status solidi B., 1975, 69 , 359-368.

56. A Taoufyq, F. Guinneton, J-C. Valmalette, M. Arab, A. Benlhachemi, B. Bakiz, S. Villain, A. Lyoussi, G. Nolibe, J-R. Gavarri, J. Solid State Chem., 2014, 219 , 127–137

57. V. O. Sokolov,V. G. Plotnichenko, E. M. Dian, Opt. Lett ., 2013, 33 , 1488-1490

58. R. Cao , M. Peng , J. Zheng , Qiu , Q. Zhang , J. Opt. Soc. Am., 2012, 16, 18505

59. B. Xu , D. Tan , S. Zhou , Z. Hong , KN. Sharafudeen , J. Qiu . J. Opt. Soc. Am., 2012, 20 (27) , 29105

60. H. Wang, F. Medina, M. S. Antonious, C. Parkanyi, J. E. Haky, D. M. Baird, and Y. D. Zhou, Chem. Phys. Lett., 1993, 205, 497-501.